RSC Advances




ROYAL SOCIETY OF CHEMISTRY

www.rsc.org/advances

# Ab Initio Study on the Excited-State Proton Transfer Mechanisms for 3-hydroxy-2-(thiophen-2-yl) chromen-4-one

Huipeng Ma*[1], Jindou Huang*[2]

[1]College of Medical Laboratory Science, Dalian Medical University, Dalian 116044, China

[2]School of Physics and Materials Engineering, Dalian Nationalities University, Dalian 116600, China

*Corresponding author: Huipeng Ma, E-mail: hpma@dlmedu.edu.cn, Tel: +86-411-86110391;

Jin-Dou Huang, E-mail: jindouhuang@dicp.ac.cn, Tel: +86-411-84379236.

**Abstract**

The optical absorption properties and fluorescence properties of 3-hydroxy-2-(thiophen-2-yl) chromen-4-one (3-HTC) were simulated by time-dependent density functional theory (TDDFT) method. The experimental absorption spectrum and fluorescence spectrum were well reproduced by calculated vertical excitation energies of 3-HTC-a that corresponds intramolecular hydrogen bond O2···H1−O1. The excited state intramolecular proton transfer (ESIPT) mechanism of 3-HTC has been systematically investigated. The constructed potential energy curves (PECs) of 3-HTC-a in the $S_0$ and $S_1$ states indicates that, after photo-excitation, the intramolecular proton transfer reaction occurs more readily with the H1 atom removing from O1 to O2 in both dynamics and thermodynamics aspects. In sharp contrast, the weak S···H1−O1 in 3-HTC-b was weakened in the $S_1$ state compared with that in the $S_0$ state, suggesting that ESIPT process is forbidden. It's the first time to find that the strong hydrogen-bond is further strengthened, and the weak hydrogen-bond is further weakened in the excited state of 3-HTC. Moreover, the vibrational frequencies of C=O and O-H groups involved in hydrogen bonds were also studied, and a more clear-cut signature of the hydrogen-bonding dynamics of 3-HTC were provided in this work.

**Introduction**

The hydrogen bond, as one of the most significant weak interactions, is ubiquitous in the natural world, which plays an important role in many branches of natural science and engineering field. It is operative in the crystallization of the material, formation of specific properties of associated liquids, and determination of the three-dimensional structures adopted by biomolecules, such likeproteins, nucleic bases and so on.[1-5] A double effect of hydrogen bond has been found in biological systems. As a collectively strong directional interaction, the hydrogen bond can lead to a relatively stable supramolecular structure, but on the other hand, it can be served as active site for initiating a plethora of chemical reactions due to the dynamic features of the proton.[5] Therefore, the intensive study of hydrogen bond interaction will be vital to elaborate many phenomenons occurring not only in the crystal packing, but also in solution and biological processes.

Actually, many different mechanism of photochemical reactions and photophysical processes can well clarify via hydrogen bonds interaction, such as intramolecular charge transfer (ICT), photo-induced electron transfer (PET), fluorescence quenching, and excited state proton transfer (ESTP), *etc*. In particular, the excited state intramolecular proton transfer (ESITP) has received enormous attention during the past half century and was revitalized recently due to its potential applications in optoelectronics, bio-imaging and sensing. ESIPT molecules possess an intramolecular hydrogen bond between the proton donor and proton acceptor, from which the proton transfer takes place upon photoexcitation, resulting in an isomer dubbed as a proton-transfer tautomer or phototautomer. Due to the drastic structural alternation, the phototautomer possesses different photophysical properties from that of the original (normal) species, offering great versatility in a variety of applications, such as lasing materials, UV photostabilizers, optical filters, radiation scintillators, molecular recognition, and so forth.[6]

As a class of typical molecules undergoing ESIPT, 3-hydroxychromoneand its derivatives (3-HCs) is a unique kind of flavonoids, composed of fused phenyl and pyranyl rings. It is mainly found in a wide variety of natural sources and is known to affect various biological processes, including the development of cancer, platelet aggregation, detoxification, and inflammatory and immune responses.[7] 3-HCs have attracted considerable interest in recent years due to their photochemistry and potential applications especially as molecular probes based on their spectrally separated dual

fluorescence.[8-13] Luthman et al. synthesized and characterized a series of 3-hydroxychromone derivatives with high fluorescent for live-cell imaging.[10] Diller et al. studied the ESIPT and photodissociation of 3‐hydroxychromone in solution, and static and femtosecond time-resolved spectroscopy were used to identify and characterize the elementary processes and intermediate states in the photocycle of 3-HC.[11] Tomin and Ushakou investigated the effect of salt ions on the ESIPT rate of 3-hydroxyflavone. The result showed that the saltions can obviously modulated intramolecular proton transfer in the excited state, and then led to increases in the short wavelength, band intensity and the fluorescence quantum yield.[12] Recently, another important intermediate 3-hydroxy-2-(thiophen-2-yl) chromen-4-one (3-HTC) was designed and reported by Chou et al.,[13] and the absorption and emission spectra were studied in acetonitrile and in relatively low polar solvents $CH_2Cl_2$ and benzene. However, spectroscopic techniques, such as time resolved fluorescence spectroscopy, provide only indirect information about the photo-physical properties and geometries. As such information is hard to extract from experiments alone, there has been a lot of effort to complement experiment by theory to better understand the mechanism and fundamental aspects concerning the hydrogen bond formation in different electronic states. Therefore, it's very urgent to study the nature of 3-HTC in detail. In order to give a clear and detailed picture of this proton transfer mechanism, in this work, we have been motivated to theoretically study the ground state and excited states of the molecule 3-HTC relevant to the hydrogen transfer mechanism using density functional theory (DFT) and time-dependent density functional theory (TDDFT) method, respectively. The geometric optimizations of 3-HTC with two types of intramolecular hydrogen bonds (O2···H1−O1 and S···H1−O1) have been performed. We further calculated and analyzed the electronic spectra, frontier molecular orbitals, homologous ground-state ($S_0$) and the first excited state ($S_1$) potential energy curves (PECs) of 3-HTC to provide direct information on the ESIPT process. Besides, the infrared spectra at both the C=O and O-H stretching vibrational regions of 3-HTC molecule was investigated as well.

**Computational Methods**

In the present work, all electronic structure calculations were carried out with the Gaussian 09 program suite.[14] Geometry optimizations of the $S_0$ state and the $S_1$ state of 3-HTC molecule were implemented using DFT method and TDDFT method. Previous studies have proven that the

TDDFT method is a useful tool to describe hydrogen bonding in the excited states of possibly hydrogen bond systems;[15-16] the Becke's three-parameter hybrid exchange functional with Lee−Yang−Parr gradient-corrected correlation (B3LYP functional)[17] and triple-zeta valence quality with one set of polarization functions (TZVP)[18] is the appropriate functional and basis set for most organic compounds.[19-22] Recently, Guerra and co-workers computationally investigated the structure and stability of DNA base pairs, and their results indicated that dispersion-corrected DFT method performed well for the hydrogen bonding and solvation e□ects in DNA.[23-25] In order to validate the accuracy of the theoretical method, a test with a series of functionals and basis sets (B3LYP/TZVP, B3LYP-D3BJ/TZVP and CAM-B3LYP/def2-qzvpd) was performed for 3-HTC-a and 3-HTC-b. For the ground state, the geometry structures optimized using B3LYP-D3BJ/TZVP is very similar to those obtained with the B3LYP/TZVP (see Table 1 and Table S1), and the UV-Vis spectra based that these structures are nearly the same, as shown in Figure 2a and Figure S1 in Supporting Information, which suggests that the dispersion effect has no obvious influence on the calculations results. Moreover, by using 3-HTC-a and 3-HTC-b as a reference set, the performance of the B3LYP/TZVP and CAM-B3LYP/def2-qzvpd was compared, and the B3LYP/TZVP results are in better agreement with the experimental reference data of Tseng et al. (see Figure 2b and Figure S2b in Supporting Information). Therefore, we selected B3LYP/TZVP in both the DFT and TDDFT calculations. The self-consistent field (SCF) convergence thresholds of the energy for both the ground state and excited state optimization were used the default setting ($10^{-6}$). Harmonic vibrational frequencies in both ground state and excited state were determined by diagonalization of the Hessian. The excited state Hessian was obtained by numerical differentiation of analytical gradients using central differences and default displacements of 0.02 Bohr. The infrared intensities were determined from the gradients of the dipole moment.[26] The geometry optimizations were performed without constraints on bond lengths, angles, or dihedral angles except constructing PESs. The S0 and S1 PESs of 3-HTC have been scanned by constrained optimizations to obtain the thermodynamic corrections in corresponding electronic state and keeping the O−H distancefixed at a series of values. All the local minima were confirmedby the absence of an imaginary mode in vibrational analysis calculations. To evaluate the solvent effect, $CH_2Cl_2$ was selected as the solvent in the calculations using the conductor-like screening model (COSMO) method [27] in the Gaussian 09 program.

## Results and Discussions

### 1. Geometric Structures

From the molecular structures of 3-HTC, we speculated that two types of intramolecular hydrogen bond might exist, that is normal hydrogen bond O2···H1−O1 and weak hydrogen bond S···H1−O1. These two types of structures were optimized using DFT and TDDFT methods in ground state and excited state, respectively. As shown in Figure 1, 3-HTC-a represent the first type of intramolecular hydrogen bond, while 3-HTC-b represent the second type of intramolecular hydrogen bond. We numerically labeled atoms connected to the hydrogen bonds to describe them more clearly. For the ground state $S_0$, the calculated bond length, bond angle and dihedral angle are listed in Table 1. The optimized results of 3-HTC-a showed that O1−H1 bond length was 0.978 Å and O2···H1 was 2.046 Å, which indicated the formation of a typical intramolecular hydrogen bond (O2···H1−O1). The inter-ring torsion angle (dihedral angle C1-C2-C3-S) of 3-HTC-a was below the measurement accuracy (< 0.1°), which suggests that the whole molecule is quasi-planar. For 3-HTC-b molecule, we can see that the bond length of O1−H1 were 0.967 Å, slightly shorter than that in 3-HTC-a, which indicates the relatively weak interaction between H atom and S atom due to lower electronegativity of S atom than O atom. The S···H distance is about 2.424 Å, which is much longer than O2···H1 bond length, but significantly shorter than the sum of van der waals radii of S and H atoms (2.90 Å). Therefore, an intramolecular hydrogen bond or analogous intramolecular hydrogen bond can be formed between S and H atoms, although this hydrogen bonding is much weaker than that of O2···H1. Besides, the inter-ring dihedral angle of 3-HTC-b is more than 10°, suggesting that the planarity of the whole molecule is significantly destroyed and it might induce a high molecular energy and poor stability compared with 3-HTC-a molecule. The energy calculations of 3-HTC-a and 3-HTC-b molecules using B3LYP/TZVP sets show that the energy of 3-HTC-b is about 10.63 kcal/mol higher than that of 3-HTC-a under vacuum condition, which is consistent with our structural analysis. It is noteworthy that the energy difference between 3-HTC-a and 3-HTC-b molecules could be effectively reduced by means of solvent effect, as discussed below.

In order to investigate the solvent effect on the intramolecular hydrogen bond and conveniently compare with available experimental results,[13] dichloromethane were used in theconductor-like screeningmodel of solvation. The related structure parameters of the stable structures are also

collected in Table 1. It can be seen that the O2−H1 length of 3-HTC-a in $CH_2Cl_2$ was changed to 2.064 Å, slightly longer than the case in vacuum. As to the 3-HTC-b, the length of S-H1 increased from 2.424 Å in vacuum to 2.455 Å in $CH_2Cl_2$. In comparison, the solvent effect of $CH_2Cl_2$ has little influence on the bond angle and inter-ring dihedral angle of 3-HTC-a and 3-HTC-b. As shown in Table 1, the variations in bond angle and dihedral angle were less than 2º. The geometry variations in 3-HTC-a and 3-HTC-b molecules indicate that the intramolecular hydrogen bond was weakened due to the effect of $CH_2Cl_2$. It may be related to the stabilization of the lone pairs involved in these bonds.[23] Furthermore, the energy of 3-HTC-a and 3-HTC-b in $CH_2Cl_2$ was calculated. It is found that the energies of 3-HTC-a and 3-HTC-b decreased by 4.87 kcal/mol and 7.82 kcal/mol, respectively, compared with the case in vacuum. It indicates that the solvent effect apparently lowered the molecular energies, especially for the molecule of 3-HTC-b. Thus, we believed that two hydrogen bonding mechanism might coexist under some extreme conditions.

The excited-state structures of 3-HTC-a and 3-HTC-b are also optimized and the related structure parameters are shown in Table 1. Comparison of geometry structures in exited state and in ground state shows that the geometry of 3-HTC-a retains their planar structures in the transition from $S_0$ to $S_1$. However, the bond length of O1−H1 becomes longer and the bond length of O2···H1 becomes shorter. In addition, the bond angle (∠O1−H···O2) of 3-HTC-a changes from 117.54°in $S_0$ state to 124.38° in $S_1$ state. Hence, the bond angle in the $S_1$ state is more close to 180° than that in the $S_0$ state. All these structural variations suggest that the intramolecular hydrogen bond O2···H1−O1 in the $S_1$ state is stronger than that in the ground state, which was consistent with the ESIPT process observed in the experiment by Chou et al.[13] Interestingly, the intramolecular hydrogen bond (S···H1−O1) of 3-HTC-b is weakened during the photo-excited process, which is quite different from the case of O2···H1−O1. As shown in Table 1, the bond length of S···H1 in 3-HTC-b changed from 2.424 Å to 2.535 Å and the angle decreased from 126.56° to 108.54°. From above analysis, we can conclude that the ESIPT process might be forbidden in the weak hydrogen bond S···H1−O1.

## 2. Electronic Spectra and Frontier Molecular Orbitals

Herein, we firstly calculated the UV-Vis absorption spectra of the 3-HTC-a and 3-HTC-b in vacuum and in $CH_2Cl_2$ solution according to the above optimized geometries. In order to validate our theoretical method, we compared the calculated absorption spectra in $CH_2Cl_2$ with the experimental

data. As shown in Figure 2a, the calculated maximum absorption band of 3-HTC-a and 3-HTC-b in $CH_2Cl_2$ located at 369 nm and 352 nm, respectively. Considering the fact that the energy of 3-HTC-a is about 7.69 kcal/mol lower than that of 3-HTC-b, we could conclude that the 3-HTC-a is the main conformation and contributes predominately to the formation of the experimental absorption spectra, and thus the calculated absorption peaks of 3-HTC-a can be used to compare with the corresponding experimental absorption peaks. Chou et al. reported that the maximum absorption band is observed in the near-UV region and is presented by the peak at 357 nm for 3-HTC in $CH_2Cl_2$, which is in agreement with our calculation results of 3-HTC-a. Moreover, the fluorescence spectrum of 3-HTC-a and 3-HTC-b are also simulated and the results are shown in Figure 2b. The excited state fluorescence maximum of 3-HTC-a is located at 405 nm, which agrees well with the weak band (~410 nm) observed in experimental observation. The red-shift of 46 nm should be ascribed to the normal Stokes shift. At the same time, another large Stokes shifted fluorescence with peak at 547 nm, which originates from the proton transfer phototautomer emission, was also found and its position is consistent with the phototautomer emission band (539 nm) determined by experiment. The much stronger emission peak located at 539 nm than the one located at 410 nm in experiment suggests that fast ESIPT takes place during photoexcitation process. For 3-HTC-b, the dual fluorescence bands will not appear in the time-resolved fluorescence spectra due to the forbidden of ESIPT. The emission maximum of 3-HTC-b is located at 347 nm, which is attributed to the normal emission, and only a very small red-shift relative to the absorption peak is observed.

To deeply understand the spectra character, the exited states and the frontier molecular orbitals (FMOs) of two types of molecular structures were analyzed in detail, which can provide information about the nature of the excited state conformations and qualitative discussion of charge distribution and charge-transfer. As shown in Table 2, our theoretical calculations show that there exists an intense $S_0 \rightarrow S_1$ transition of 3-HTC-a at 369.24 nm with oscillator strength of 0.4345. The first singlet excited ($S_1$) states of 3-HTC-a is dominantly formed by the transitions from the highest occupied molecular orbital (HOMO) to the lowest unoccupied molecular orbital (LUMO). The HOMO and LUMO of 3-HTC-a are shown in Figure 3a. It is evident that the HOMO distribution localized on hydrogen bond O2···H1−O1 is quite different from the LUMO distribution. This difference indicates that the $S_1$ state corresponding to the HOMO-LUMO transition should have intramolecular charge-transfer (ICT). Further analysis of these FMOs in

Figure 3a shows that O1−H1 bond contribute to the HOMO in a bonding fashion, while the LUMO localized on the O1−H1 bond has a strong nonbonding character. This variation of charge distribution inevitably induces changes in bond order and bond length alteration. According the relationship between local bonding characters and bond order,[28] it is easy to understand the increase of O1−H1 bond length in the exited state. Also, the charge distribution localized on C=O changes slightly during photo-excitation process. As shown in Figure 3a, the percentage of antibonding character is obviously larger in LUMO than in HOMO, which contribute to the longer C=O bond length in $S_1$ state than that in $S_0$ state. In addition, it should be noted that the H1 atom was completely naked in the $S_1$ state, which effectively improves its electron-accepting ability, and thus the interaction between H1 and O2 atom is enhanced after photoexcitation to the S1 state. Our analysis of the shape of FMOs here well rationalizes the hydrogen bond enhancement in exited state.

Meanwhile, the molecular orbitals of 3-HTC-b have also been calculated and the shapes of the FMOs are shown in Figure 3b. It can be seen that an intense $S_0 \rightarrow S_1$ transition for 3-HTC-b is predicted at about 352 nm with large oscillator strength of 0.4407, the specific information can be found in Table 2. Similar with 3-HTC-a, $S_0 \rightarrow S_1$ transition can be described as a predominantly $\pi\pi^*$-type transition from HOMO to LOMO. From Figure 3b, we can also see that the HOMO localized on the C2-C3 bond shows a strong antibonding character, while the LUMO shows an obvious bonding character, which suggests that C2 and C3 are inclined to form single bond in the ground state and to form double bond in the exited state. It well explains the larger dihedral angles (**C1-C2-C3-S**) in the ground state (28.57º) than that in the exited state (12.90º). Moreover, it should be noted that there is a vertical node at right angles in the LUMO localized on the S···H1−O1, which increases the distances between S and O1, and thus the hydrogen bond S···H1−O1 is weakened to some extent.

### 3. Potential Energy Curves

It's an effective method to construct the potential curve for investigating the molecular properties and hydrogen transfer reactions, and PECs could provide more intuitive information about the ESIPT process. Herein, the calculation of PECs are performed using the constrained optimizations in the $S_0$ state and $S_1$ state geometrical structures along with the fixed O1−H1 bond length at the

DFT/B3LYP/TZVP level. The constructed PECs in the $S_0$ and $S_1$ states as functions of the O1−H1 length fixed at values in the range from 0.96 Å to 2.5 Å (see Figure 4). Previous work has indicated that the TDDFT/B3LYP method was reliable for the determination of qualitative energetic pathways for intramolecular proton-transfer process, even though it may not be expected to be sufficiently accurate in yielding the correct ordering of the closely spaced excited states.[15-16,19-22]

As shown in Figure 4, we can see clearly that the energy of $S_0$ state increases along with lengthening of the O1−H1 bond from its stable structure, producing a potential barrier of 13.31 kcal/mol. It indicates that the ground state intramolecular proton transfer (GSIPT) process is difficult to happen due to the high potential barrier in the process of the proton H1 transferring from O1 to O2. In terms of thermodynamics, GSIPT of 3-HTC-a is an endothermic reaction and $\Delta H$=10.63 kcal/mol, which indicates that the energy of molecular system is improved 10.63kcal/mol after the process of the proton H1 transferring from O1 to O2 in the $S_0$ state. Therefore, it is unfavorable for the GSIPT process from the point of dynamics and thermodynamics. In comparison, it exhibits a barrier of only 2.96 kcal/mol between the excited state equilibrium geometry of 3-HTC-a and its stable proton transfer phototautomer. So, we can conclude that the intramolecular proton transfer process of the 3-HTC is more likely to happen in the $S_1$ state from the view of dynamics. Also, ESIPT process is an exothermic reaction and the energy of the molecular systems decreased by 9.20 kcal/mol after the process of the proton H1 transferring from O1 to O2. Therefore, the intramolecular proton transfer can easily happen in the excited state.

## 4. Infrared Spectra

It is well known that the vibrational frequencies of the stretching vibrationsof C=O and O-H groups involved in hydrogen bonds can provide a clear-cut signature of the hydrogen-bonding dynamics. Herein, the infrared spectra (IR) spectra of 3-HTC inthe ground state ($S_0$) and in single excited-state ($S_1$) are calculated using TDDFT method. The vibrational spectra of 3-HTC in the conjunct vibrational regions of the O-H and C=O stretching modes can be seen in Figure 4. The calculated O1−H1 stretching vibrational frequency of the molecule 3-HTC-a in the $S_0$ state is located at 3583 $cm^{-1}$, and it moves to 3176 $cm^{-1}$ in the $S_1$ state. A strong red-shift of 407 $cm^{-1}$ for

the O1−H1 stretching band can be driven by changes of local charge distribution, since the electronic state hopping from $S_0$ state to the S1 state is followed by the intramolecular charge redistribution in the $S_1$ state of 3-HTC-a, as discussed in the part **Electronic Spectra and Frontier Molecular Orbitals.**

For the molecule of 3-HTC-b, the vibration mode of the intramolecular hydrogen bond O1−H1 is blue shifted from 3753 $cm^{-1}$ at $S_1$ state, respectively, to 3740 $cm^{-1}$ at $S_0$ state, which is opposite with the previous changes of O1−H1 stretching band in 3-HTC-a. According to the effective rule for verifying the changes of hydrogen bond in the excited state proposed by Han,[4,29-30] we can conclude that the intramolecular hydrogen bonds O1−H1···O2 is strengthened in the excited state through an electronic spectral redshift and the intramolecular hydrogen bond O1−H1···S is weakened at excited state through an electronic spectral blueshift. The conclusion is consistent with our frontal structural analysis.

For the convenience of our discussion about the influence of hydrogen bond on the vibrational mode of C=O bond, the infrared spectra of C=O bonds in the molecules of 3-HTC-a and 3-HTC-b are investigated for comparison. As shown in Figure 4, we can clearly find that the calculated C=O stretching vibrational frequency in the $S_0$ state is located at 1715 $cm^{-1}$ in the molecule 3-HTC-b, and it changes to be 1682 $cm^{-1}$ and 1657 $cm^{-1}$ in the 3-HTC-a due to the formation of intramolecular hydrogen bond (O1−H1···O2). It indicates that the hydrogen bond could effectively weaken the bond order of C=O due to the strong interaction between H1···O2, as also can be seen from the slightly longer C=O bond length in 3-HTC-a (1.24 Å) than the one in 3-HTC-b (1.22Å). According Hooke's rule $\nu = \frac{1}{2\pi c}\sqrt{\frac{k}{\mu}}$ ($c$ denotes velocity of light, $k$ denotes the force constant, and $\mu$ denotes the reduced mass), it is easy to understand the observation that the vibration frequency redshift with the decrease of the force constant of the carbonyl. Furthermore, we also analyzed the influence of different electronic state on the vibrational mode of C=O bond. As shown in Figure 4, the calculated C=O stretching vibrational frequency in the $S_1$ state is located at 1611 $cm^{-1}$ and 1654 $cm^{-1}$, separately, corresponding the symmetric and antisymmetric stretching vibration in 3-HTC-a, which is strongly upshifted by 46 $cm^{-1}$ and 28 $cm^{-1}$, compared with the one in the $S_0$ state, respectively. That is to say, the C=O stretching mode has a large redshift which is induced by the intramolecular hydrogen bond

strengthening in the excited state. It is consistent with the previous analysis result that the hydrogen bond is strengthened in the exited state.

**Conclusion**

In summary, the optical absorption properties and fluorescence properties 3-HTC were systematically investigated by time-dependent density functional theory method. The experimental absorption spectrum was well reproduced by calculated vertical excitation energies of 3-HTC-a that corresponds intramolecular hydrogen bonds O2···H1-O1. Also, we predicted the dual fluorescence behavior of the fluorescence spectrum of 3-HTC, which is in good agreement with experimental results. One of the fluorescence maxima at 405 nm (~410 nm) is attributed to normal emission; and the other one of fluorescence maxima at 547 nm (539 nm) originates from the proton transfer phototautomer emission. The excited state intramolecular proton transfer (ESIPT) mechanism of 3-HTC have been investigated in detail. Upon excitation, the intramolecular hydrogen bonds O2···H1-O1 was significantly strengthened in the $S_1$ state, which provides a driving force in facilitating the proton transfer process effectively. The constructed potential energy curves (PECs) of 3-HTC-a in the $S_0$ and $S_1$ states further confirms that, after photo-excitation, the IPT reaction occurs more readily with the H1 atom removing from O1 to O2 in both dynamics and thermodynamics aspects. In sharp contrast, the weak hydrogen bond S···H1-O1 in 3-HTC-b was weakened in the $S_1$ state compared with that in the $S_0$ state, suggesting that ESIPT process is forbidden. It's the first time to find that the strong hydrogen-bond is further strengthened and the weak hydrogen-bond is further weakened in the excited state of 3-HTC. Based on the FMOs analysis, the local bonding character correlated with the local structural adjustment were discussed, which rationalizes the changes in hydrogen bonds and geometric structures of 3-HTC. Moreover, the vibrational frequencies of C=O and O-H groups involved in hydrogen bonds were also studied, and a more clear-cut signature of the hydrogen-bonding dynamics of 3-HTC were provided in this work.

Acknowledgements

This work was supported by the National Science Foundation of China (Grant No. 21503034, 81601825), Fundamental Research Funds for the Central Universities (Grant No. DC15013705),

Program for Science and Technology Project of Liaoning Province (Grant No. 201601237), Educational Committee Foundation of Liaoning Province (Grant No. L2015150), and the Initial Funds for Imported Talents' Research Projects, Dalian Nationalities University (Grant No. 20136131).

## References

**1.** A. G. Slater, L. M. A. Perdigao, P. H. Beton and N. R. Champness, Acc. Chem. Res., 2014, **47**, 3417-3427.

**2.** Y. Takezawa and M. Shionoya, Acc. Chem. Res., 2012, **45**, 2066-2076.

**3.** M. Egli, Acc. Chem. Res., 2012, **45**, 1237-1246.

**4.** G.-J. Zhao and K.-L. Han, Acc. Chem. Res., 2012, **45**, 404-413.

**5.** L. Sobczyk, S. J. Grabowski and T. M. Krygowski, Chem. Rev., 2005, **105**, 3513-3560.

**6.** V. S. Padalkar and S. Seki, Chem. Soc. Rev., 2016, **45**, 169-202.

**7.** S. Gunduz, A. C. Goren and T. Ozturk, Org. Lett., 2012, **14**, 1576-1579.

**8.** S. Basu, S. Mondal and D. Mandal, J. Chem. Phys., 2010, **132**.

**9.** A. P. Demchenko, K.-C. Tang and P.-T. Chou, Chem. Soc. Rev., 2013, **42**, 1379-1408.

**10.** C. Dyrager, A. Friberg, K. Dahlen, M. Friden-Saxin, K. Borjesson, L. M. Wilhelmsson, M. Smedh, M. Grotli and K. Luthman, Chem. Eur. J., 2009, **15**, 9417-9423.

**11.** K. Chevalier, A. Gruen, A. Stamm, Y. Schmitt, M. Gerhards and R. Dillert, J. Phys. Chem. A, 2013, **117**, 11233-11245.

**12.** V. I. Tomin and D. V. Ushakou, J. Appl. Spectrosc., 2015, **82**, 193-199.

**13.** H.-W. Tseng, J.-Y. Shen, T.-Y. Kuo, T.-S. Tu, Y.-A. Chen, A. P. Demchenko and P.-T. Chou, Chem. Sci., 2016, **7**, 655-665.

**14.** G. W. T. M. J. Frisch, H. B. Schlegel, G. E. Scuseria, M. A. Robb, J. R. Cheeseman, G. Scalmani, V. Barone, B. Mennucci, G. A. Petersson, H. Nakatsuji, M. Caricato, X. Li, H. P. Hratchian, A. F. Izmaylov, J. Bloino, G. Zheng, J. L. Sonnenberg, M. Hada, M. Ehara, K. Toyota, R. Fukuda, J. Hasegawa, M. Ishida, T. Nakajima, Y. Honda, O. Kitao, H. Nakai, T. Vreven, J. A. Montgomery, Jr., J. E. Peralta, F. Ogliaro, M. Bearpark, J. J. Heyd, E. Brothers, K. N. Kudin, V. N. Staroverov, R. Kobayashi, J. Normand, K. Raghavachari, A. Rendell, J. C. Burant, S. S. Iyengar, J. Tomasi, M. Cossi, N. Rega, J. M. Millam, M. Klene, J. E. Knox, J. B. Cross, V. Bakken, C. Adamo, J. Jaramillo, R. Gomperts, R. E. Stratmann, O. Yazyev, A. J. Austin, R. Cammi, C. Pomelli, J. W. Ochterski, R. L. Martin, K. Morokuma, V. G. Zakrzewski, G. A. Voth, P. Salvador, J. J. Dannenberg, S. Dapprich, A. D. Daniels, Ö. Farkas, J. B. Foresman, J. V. Ortiz, J. Cioslowski, and D. J. Fox, Gaussian 09, Revision E.01, Gaussian, Inc., Wallingford CT, 2009.

**15.** G.-Y. Li and T. Chu, Phys. Chem. Chem. Phys., 2011, **13**, 20766-20771.

**16.** G.-Y. Li, G.-J. Zhao, Y.-H. Liu, K.-L. Han and G.-Z. He, J. Comput. Chem., 2010, **31**, 1759-1765.

**17.** C. T. Lee, W. T. Yang and R. G. Parr, Phys. Rev. B, 1988, **37**, 785-789.

**18.** O. Treutler and R. Ahlrichs, J. Chem. Phys., 1995, **102**, 346-354.

**19.** J. Zhao, J. Chen, Y. Cui, J. Wang, L. Xia, Y. Dai, P. Song and F. Ma, Phys. Chem. Chem. Phys., 2015, **17**, 1142-1150.

**20.** J. Zhao, J. Chen, J. Liu and M. R. Hoffmann, Phys. Chem. Chem. Phys., 2015, **17**, 11990-11999.

**21.** J. Zhao and P. Li, Rsc Adv., 2015, **5**, 73619-73625.

**22.** J. Zhao, H. Yao, J. Liu and M. R. Hoffmann, J. Phys. Chem. A, 2015, **119**, 681-688.

**23.** J. Poater, M. Swart, C. F. Guerra and F. M. Bickelhaupt, Comput. Theor. Chem., 2012, **998**, 57-63.

**24.** J. Poater, M. Swart, F. M. Bickelhaupt and C. F. Guerra, Org. Biomol. Chem., 2014, **12**, 4691-4700.

**25.** J. Poater, M. Swart, C. F. Guerra and F. M. Bickelhaupt, Chem. Commun., 2011, **47**, 7326-7328.

**26.** F. Furche and R. Ahlrichs, J. Chem. Phys., 2002, **117**, 7433-7447.

**27.** A. Klamt and G. Schuurmann, J. Chem. Soc. Perk. T. 2, 1993, 799-805.

**28.** Y. C. Chang and I. Chao, J. Phys. Chem. Lett., 2010, **1**, 116-121.

**29.** G.-J. Zhao and K.-L. Han, J. Phys. Chem. A, 2007, **111**, 2469-2474.

**30.** G.-J. Zhao and K.-L. Han, Biophys. J., 2008, **94**, 38-46.

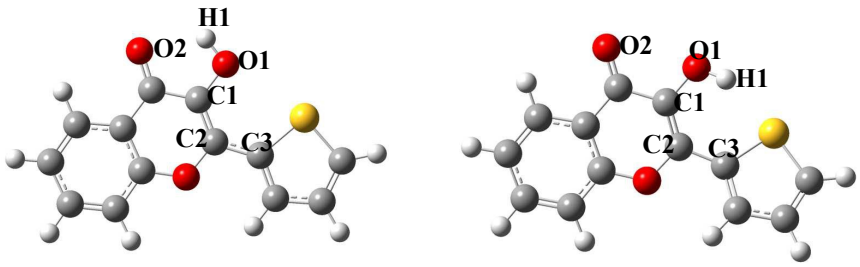


3-HTC-a 3-HTC-b

Figure1. Optimized structures of 3-HTC-a and 3-HTC-b.

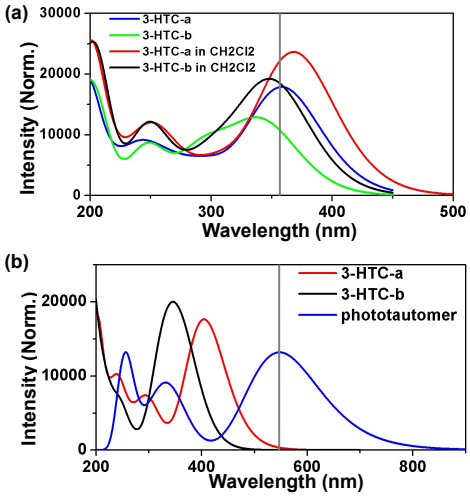


Figure 2. (a) Calculated UV-Vis absorption spectra of 3-HTC-a and 3-HTC-b in vacuum (blue and green lines) and in $CH_2Cl_2$ (red and black lines); (b) the fluorescence spectra of 3-HTC-a (red line), phototautomer of 3-HTC-a (blue line), and 3-HTC-b (black line) based on B3LYP/TZVP level; and the cross vertical line shows the experimental data in $CH_2Cl_2$.

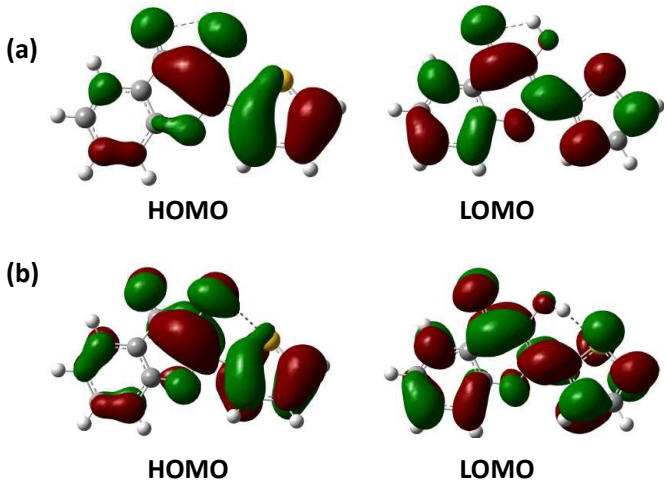


Figure 3. HOMO and LOMO features of 3-HTC-a and 3-HTC-b obtained from DFT/B3LYP/TZVP calculations, respectively.

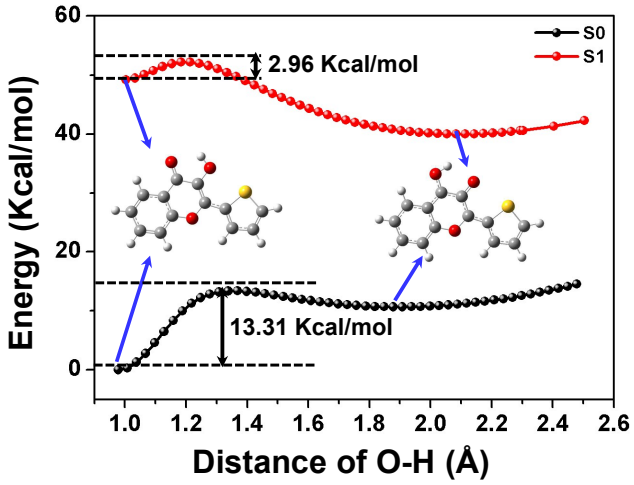


Figure.4 Potential energy curves of $S_0$ and $S_1$ states of 3-HTC-a as a function of O-H bond length.

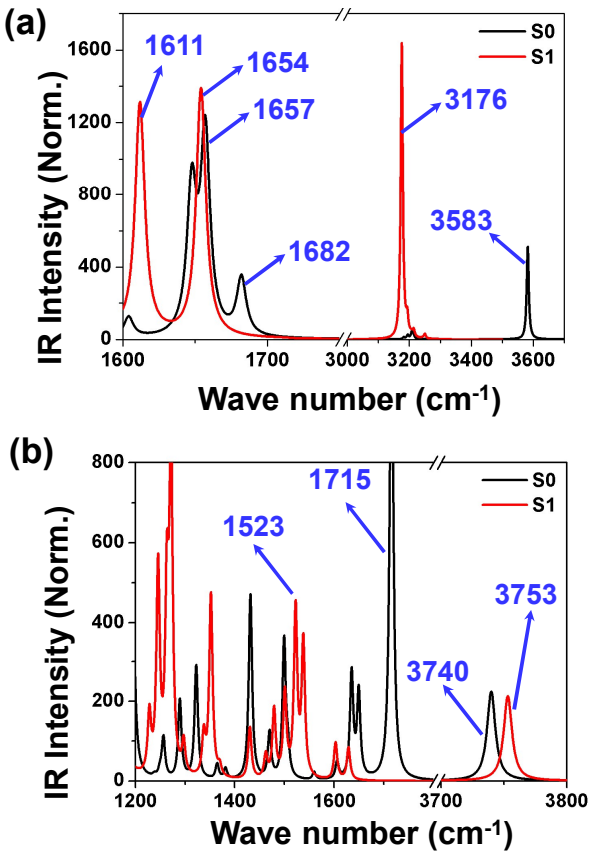


Figure. 5 The calculated IR spectra of 3-HTC-a (a) and 3-HTC-b (b) for the ground state ($S_0$) and single excited-state ($S_1$) in the spectral region of the O-H and C=O strengthening bands.

Table 1 Calculated Bond lengths (Å), angles and dihedral angles of 3-HTC-a and 3-HTC-b structures of the $S_0$ state in vacuum and in $CH_2Cl_2$, as well as $S_1$ states in vacuum at B3LYP/TZVP level.

| **Molecules** | **O1-H1** | | **O2-H1** | | **S-H1** | | **O1-H1-O2/S** | | **C1-C2-C3-S** | |
|---|---|---|---|---|---|---|---|---|---|---|
| | $S_0$ | $S_1$ | $S_0$ | $S_1$ | $S_0$ | $S_1$ | $S_0$ | $S_1$ | $S_0$ | $S_1$ |
| **3-HTC-a** | 0.978 | 1.003 | 2.046 | 1.831 | 3.832 | 3.935 | 117.5 | 124.4 | 0.0 | 0.0 |
| **3-HTC-b** | 0.967 | 0.967 | 3.627 | 3.516 | 2.424 | 2.535 | 126.6 | 108.5 | 28.6 | 12.9 |
| **3-HTC-a($CH_2Cl_2$)** | 0.977 | — | 2.064 | — | 3.831 | — | 116.8 | — | 0.0 | — |
| **3-HTC-b($CH_2Cl_2$)** | 0.968 | — | 3.622 | — | 2.455 | — | 125.0 | — | 30.5 | — |

Table 2. Electronic excitation energy (nm), oscillator strengths, and the corresponding compositions for 3-HTC-a and 3-HTC-b in vacuum and in $CH_2Cl_2$, and for phototautomer of 3-HTC-a in vacuum.

| | transition | λ (nm) | *f* | composition | CI |
|---|---|---|---|---|---|
| 3-HTC-a | $S_0 \rightarrow S_1$ | 359.4 | 0.4345 | H→L | 96.9% |
| Phototautomer of 3-HTC-a | $S_0 \rightarrow S_1$ | 547.2 | 0.3258 | H→L | 100% |
| | $S_0 \rightarrow S_3$ | 348.7 | 0.1388 | H-2→L | 81.5% |
| 3-HTC-b | $S_0 \rightarrow S_2$ | 342.8 | 0.2630 | H→L | 83.7% |
| | $S_0 \rightarrow S_3$ | 295.9 | 0.1993 | H-1→L | 47.5% |
| | | | | H-2→L | 48.2% |
| | $S_0 \rightarrow S_8$ | 251.6 | 0.1104 | H→L+2 | 81.8% |
| 3-HTC-a ($CH_2Cl_2$) | $S_0 \rightarrow S_1$ | 369.2 | 0.5750 | H→L | 97.9% |
| | $S_0 \rightarrow S_2$ | 308.7 | 0.1274 | H-1→L | 95.4% |
| 3-HTC-b($CH_2Cl_2$) | $S_0 \rightarrow S_1$ | 352.0 | 0.4407 | H→L | 97.1% |
| | $S_0 \rightarrow S_3$ | 303.1 | 0.1833 | H-1→L | 93.8% |